J Therm Anal Calorim (2011) 105:995–1006
DOI 10.1007/s10973-011-1539-0

Synthesis and properties of novel ferroelectric liquid crystalline polyacetylenes containing terphenyl mesogens with chiral groups

Ting Hu · Huanling Kong · Lie Chen · Yiwang Chen · Fan Li · Daijun Zha

Received: 8 November 2010 / Accepted: 29 March 2011 / Published online: 12 April 2011

Abstract Novel ferroelectric liquid crystalline (FLC) polyacetylenes, namely, "side-end-fixed" type of **PAM$_6$O-TPhOR*** and "side-on-fixed" type of **PAM$_3$OCO(TPh)OR*** were designed and synthesized in high yields (89.3 and 62.0%), respectively, where the terphenyl was linked at the different positions. The thermal stability of **PAM$_3$OCO(TPh)OR*** is better than **PAM$_6$OTPhOR*** owing to the "jacket effect" from terphenyl pendant linked at the waist position well protecting the main chain from the perturbations. The **PAM$_3$OCO(TPh)OR*** shows enantiotropic chiral smectic A phase (SmA*), but it is noteworthy that the **PAM$_6$OTPhOR*** exhibits enantiotropic chiral smectic C phase (SmC*) responsible for ferroelectric liquid crystallinity. Compared to "side-end-fixed" type of polymer, the "side-on-fixed" type shows better light emitting property, ascribed to the mesogen linked at the waist position has stronger tendency to enhance the main-chain coplanarity. Furthermore, the circular dichroism (CD) spectra demonstrate that the asymmetric force field generated by the chiral center affects the secondary structure of **PAM$_3$OCO(TPh)OR***.

Keywords Polyacetylene · Ferroelectric liquid crystalline · Terphenyl · Photoluminescence

T. Hu · H. Kong · L. Chen (✉) · Y. Chen (✉)
Department of Chemistry, Nanchang University, 999 Xuefu Avenue, Nanchang 330031, China
e-mail: chenlienc@163.com

Y. Chen
e-mail: ywchen@ncu.edu.cn

T. Hu · L. Chen · Y. Chen · F. Li (✉) · D. Zha
Institute of Polymers, Nanchang University, 999 Xuefu Avenue, Nanchang 330031, China
e-mail: lfan@ncu.edu.cn

Introduction

It is well known that liquid crystals (LC) play an important role in modern optical technology. π-Conjugated polymers are widely used in the fields of thin film transistors, light-emitting diodes [1, 2]. Melding of the two at molecular level may generate liquid crystalline conjugated polymers (LCCPs) with novel optical and electronic activities. Because of the orientability of the mesogens by external forces, the polymers may exhibit both linearly [3] and circularly polarized emissions [4] which have been employed to impart new features to electrochromic systems [5]. The liquid crystalline conjugated polyacetylene (LCCPA) has attracted much synthetic effort over the past decades, due to its unique characteristics such as semiconductivity, high gas permeability, helix inversion, and nonlinear optical properties [6].

Among the LCCPs, side-chain liquid crystalline conjugated polymers (SCLCCPs) are most popular. According to the position in which the mesogens are attached to the conjugated backbones, SCLCCPs can be divided into two categories. One has mesogens linked at the end position (side-end-fixed), and the other has mesogens linked at the waist or mass center position (side-on-fixed). Many research groups are mainly concentrated on the side-end-fixed type mesomorphic conjugated polymers [7–10]. The concept of side-on-fixed polymer was first proposed by Zhou [11]. So far, most side-on-fixed polymers synthesized are flexible main chain polymers, and few side-on-fixed conjugated polymers have been studied except the recent reports [10, 12].

When an electric field is employed as an external force, ferroelectric liquid crystalline (FLC) are more desirable than ordinary LC ones because the former are expected to respond more quickly to the electric field owing to their

spontaneous polarization, than the latter. The FLC is due to spontaneous polarization generated in the chiral smectic C phase (SmC*) when it is surface stabilized. One of the promising approaches to obtain FLC is to include a chiral center to the LCCPs. Up to now, some conjugated polymers including mono-substituted polyacetylene [13, 14], polythiophene [15], poly(*para*-phenylenevinylene) derivative [16], and polyphenylene derivatives [17] with chiral LC side chains were synthesized along with this strategy. But the difficulty to generate SmC* phase responsible for ferroelectric liquid crystallinity may result in neither quick electroresponsive behavior nor the switching function based on polarization inversion has been achieved.

The terphenyl is not only a chromophore but also a mesogenic core [18, 19]. In our previous study [10], we have synthesized a series of LCCPAs containing terphenyl mesogens, and found that the molecules could not only be easily aligned by spontaneous orientation of the LC group, but also the energy could be transferred from mesogens to main chain to favor the fluorescence efficiency. This encouraged us to extend our investigations to design FLC conjugated polyacetylenes (FLCCPAs) containing terphenyl mesogenic pendants with chiral center and check how the structural variations exert their effect on the properties. In this study, we synthesized two types (side-end-fixed and side-on-fixed) of side-chain FLCCPAs containing terphenyl mesogens with (*S*)-2-methylbutyl chiroptical end groups (Scheme 1). This article reports the details of synthesis and characterization of the monomers and their polymers. Also special attention was paid to the effects of terphenyl mesogens and chiroptical end groups on the properties of the products.

Experimental

Materials

The *n*-butyllithium (*n*-BuLi) (2.72 M in hexane, packaged under Argon in resealable), trimethyl borate ($B(OCH_3)_3$), 2,5-dibromotoluene, 4-bromo-4′-hydroxybiphenyl, *p*-bromoanisole, 4-pentyn-1-ol, tetrakis(triphenylphosphine)palladium(0) ($[Pd(PPh_3)_4]$), 4-bromophenol, diethyl azodicarboxylate (DEAD, 40% in toluene), $[Rh(nbd)Cl]_2$ were purchased from Alfa Aesar. 1,6-Dibromehexane, sodium acetylide (18 wt% in xylene) were purchased from Aldrich. (*S*)-2-Methyl-1-butanol was purchased from Tokyo Kasei (TCI), and used as received without any further purification. Tetrahydrofuran (THF) was dried over sodium [12], Et_3N and dichloromethane (CH_2Cl_2) were dried over calcium hydride and then distilled under nitrogen. Other chemicals were used as received from Sinopharm Chemical Reagent Co. Ltd (SCRC).

Techniques

Melting point was measured on a XT-4A apparatus. The nuclear magnetic resonance (NMR) spectra were recorded on a Bruker ARX 600 NMR spectrometer with deuterated chloroform as the solvent and TMS was used as an internal standard. Infrared spectroscopic measurements were recorded on a Shimadzu IRPrestige-21 Fourier transform infrared (FTIR) spectrophotometer using KBr substrates. The UV spectra of the samples were collected on a Hitachi UV-2300 spectrophotometer. Fluorescence measurements for photoluminescence (PL) of the polymer were carried out on a Shimadzu RF-5301 PC spectrofluorophotometer with a xenon lamp as the light source. Optical texture observations were performed with a Nikon E600POL polarizing optical microscope equipped with an Instec HS 400 heating and cooling stage. Thermogravimetric analysis (TG) (Aluminum Oxide crucible, 75 μL) was performed on a PerkinElmer TGA 7 for thermogravimetry at a heating rate of 10 °C min^{-1} under nitrogen. Differential scanning calorimetry (DSC) (Aluminum crucible, 5.4 × 2.7 mm) was used to determine phase-transition temperatures on a Shimadzu DSC-60 with a heating/cooling rate of 10 °C min^{-1} with a sample size of 3–5 mg. The X-ray diffraction (XRD) study of the samples were carried out on a Bruker D8 Focus X-ray diffractometer operating at 30 kV and 20 mA with a copper target ($\lambda = 1.54$ Å) and at a scanning rate of 1° min^{-1}. The gel permeation chromatography (GPC) was conducted with a Breeze Waters system equipped with a Rheodyne injector, a 1515 Isocratic pump, and a Waters 2414 differential refractometer using polystyrenes as the standard and chloroform ($CHCl_3$) as the eluent at a flow rate of 1.0 mL min^{-1} and 40 °C through a Styragel column set, Styragel HT3, and HT4 (19 mm × 300 mm, $10^3 + 10^4$ Å) to separate molecular weight (MW) ranging from 10^2 to 10^6. The circular dichroism (CD) spectra were conducted using a MOS-450/AF-CD apparatus.

Synthesis of the monomers

The synthesis and structures of the monomers are outlined in Scheme 1. All of the reactions and manipulations were carried out under nitrogen except the oxidation reaction.

8-Bromo-1-octyne

A solution of sodium acetylide (44 g, 18 wt% in xylene, 0.16 mol) was very slowly added to a solution of 1,6-dibromohexane (120 g, 0.49 mol) in 60 mL of *N*,*N*-dimethylformamide (DMF) by pressure-equalized dropping funnel. The reaction mixture was refluxed for 24 h at 50 °C. The precipitate was removed by filtration, and the solvent

Scheme 1 Illustration of procedures for synthesis of **AM$_6$OTPhOR***, **PAM$_6$OTPhOR***, **AM$_3$OCO(TPh)OR***, and **PAM$_3$OCO(TPh)OR***

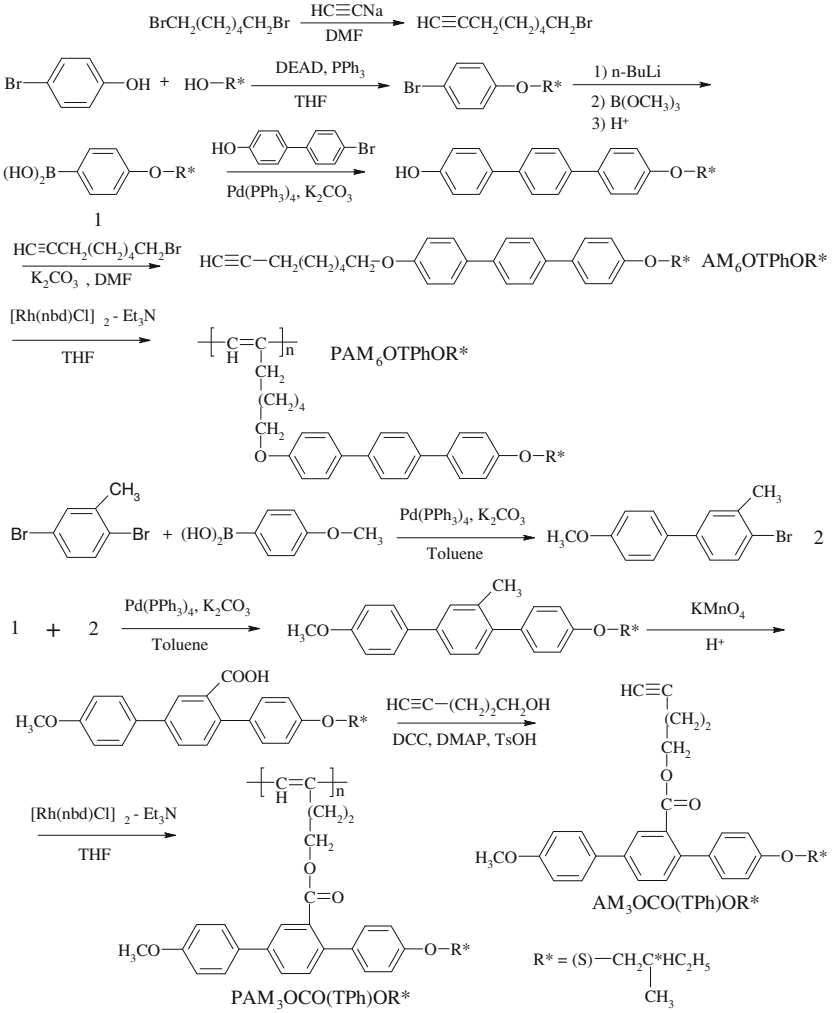

was evaporated. Vacuum distillation afforded 20.2 g of colorless oily product (60–62 °C/88 Pa). Yield: 66.01%. IR (KBr, cm^{-1}): ν 3301 (≡C–H), 2116 (C≡C), 637 (≡C–H bending). ^{1}H NMR (600 MHz, $CDCl_3$-*d*, ppm): 1.43–1.54 (m, 6H, ≡CCH$_2$C*H$_2$*C*H$_2$*C*H$_2$*), 1.86 (t, 1H, *HC*≡), 2.18 (m, 2H, HC≡CC*H$_2$*), 2.81 (m, 2H, C*H$_2$*CH$_2$Br), 3.42 (t, 2H, C*H$_2$*Br).

4-Bromo-4′-((S)-2-methylbutyl)oxybenzene

A solution of 4-bromophenol (6.92 g, 40 mmol) and DEAD (17.4 g, 20 mmol, 18 wt% in toluene) in 40 mL of THF was added to a solution of triphenylphosphine (TPP) (10.6 g, 40 mmol) and (*S*)-2-methyl-1-butanol (2.65 g, 30 mmol) in THF (50 mL) by a pressure-equalized dropping funnel. After completion of the addition, the solution was stirred for 24 h. Then the solvent was evaporated, and the crude product was purified by column chromatography (silica gel, *n*-hexane/ethyl acetate = 8). The product was obtained as colorless oily liquid. Yield: 70.0%. ^{1}H NMR (600 MHz, $CDCl_3$-*d*, δ, ppm): 0.93–0.95 (t, 3H, –OCH$_2$CHCH$_2$–C*H$_3$*). 0.98–1.00 (d, 3H, –OCH$_2$CH–C*H$_3$*), 1.24–1.28 (m, 2H, –OCH$_2$CH(CH$_3$)–*CH$_2$*), 1.70–1.80 (m, 1H, –OCH$_2$–C*H*), 3.68–3.76 (d, 2H, –OC*H$_2$*–CH), 6.75–6.77 (d, 2H, Ar–*H*), 7.33–7.35 (d, 2H, Ar–*H*).

4-((S)-2-Methylbutyl)oxyphenylboronic acid

4-Bromo-4′-((*S*)-2-methylbutyl)oxybenzene (2.43 g,10 mmol) was dissolved in 30 mL of anhydrous THF in a 250 mL three-neck flask equipped with a pressure-equalized dropping funnel. The solution was cooled to −78 °C with the bath of liquid nitrogen–acetone. The *n*-BuLi (4.4 mL, 0.012 mol, 2.72 M in hexane) was added dropwise to the stirring mixture slowly, maintaining the temperature below −78 °C. After 1 h, $B(OCH_3)_3$ (1.36 mL, 12 mmol) in 5.2 mL of anhydrous THF was added dropwise to the stirring mixture. The reaction mixture was subsequently warmed to room

temperature and stirred overnight, then 7.5 mL 5% dilute HCl was added dropwise, and the mixture was stirred for 1 h. Finally, the mixture was extracted three times with ether, washed with water. The organic layer was combined and dried over anhydrous magnesium sulfate ($MgSO_4$) over night and filtered. After the evaporation of the solvent, the white powder was dissolved in THF, precipitated in hexane, and filtered to yield a white powder. Yield: 67.2%. M.p.: 109–111 °C.

4-Hydroxy-4′-((S)-2-methylbutyl)oxy-p-terphenyl

Into a 250 mL three-necked, round-bottom flask, 4-bromo-4′-hydroxybiphenyl (2.49 g, 0.01 mol), $Pd(PPh_3)_4$ (0.192 g), potassium carbonate (K_2CO_3) (1.38 g, 0.01 mmol), H_2O (9 mL), toluene (12 mL) were added under the protection of nitrogen, 4-((*S*)-2-methylbutyl)oxylphenylboronic acid (2.5 g, 0.012 mol) dissolved in 9 mL of ethanol was added dropwise at 80 °C. The reaction mixture was stirred overnight. Then the mixture was extracted with chloroform ($CHCl_3$) and water. The organic layer was separated, dried over anhydrous $MgSO_4$, and filtered, then the solvent was distilled with a rotary evaporator and the resulting mixture was purified by column chromatography (silica gel, *n*-hexane/dichloromethane = 5). White crystals were afforded. Yield: 63.2%. M.p.: 230–232 °C. ^{1}H NMR (600 MHz, $CDCl_3$-*d*, δ, ppm): 0.89–0.91 (t, 3H, –OCH_2CHCH_2–CH_3), 0.96–0.97 (d, 3H, –OCH_2CH–CH_3), 1.18–1.23 (–$OCH_2CH(CH_3)CH_2$) 1.70–1.80 (m, 1H, –OCH_2–C*H*), 3.71–3.79 (d, 2H, –OCH_2–CH), 6.84–6.86 (d, 2H, Ar–*H*), 6.91–6.93 (d, 2H, Ar–*H*), 7.45–7.53 (d, 8H, Ar–*H*).

*8-[(4′-((S)-2-Methylbutyloxy)-4-terphenyl)oxy]-1-octyne (**AM$_6$OTPhOR***)*

Under the protection of nitrogen, 4-hydroxy-4′-((*S*)-2-methylbutyl)oxyl-*p*-terphenyl (1.66 g, 0.0050 mol), 8-bromo-1-octyne (1.42 g, 0.0075 mol), K_2CO_3 (1.12 g, 0.012 mol), KI (0.083 g, 0.5 mmol), DMF (75 mL) was stirred for 24 h at 90 °C. After the mixture had cooled to room temperature, the solution was filtered off, and the filtrate was evaporated under vacuum. White power was afforded by recrystallization from $CHCl_3$. Yield: 54.5%. IR (KBr, ν, cm^{-1}): 2111 (C≡C), 3282 (≡CH). ^{1}H NMR (600 MHz, $CDCl_3$-*d*, δ, ppm): 0.95–0.97 (t, 3H, –OCH_2-$CHCH_2$–CH_3), 0.99–1.05 (d, 3H, –OCH_2CH–CH_3), 1.25–1.30 (m, 2H, –$OCH_2CH(CH_3)$–CH_2), 1.52–1.96 (m, 9H, –CH_2(CH_2)$_4$$CH_2$–, *H*C≡), 2.21–2.22 (m, 3H, –OCH_2–C*H*, ≡CCH_2), 3.77–4.00 (d, 2H, –OCH_2–$CHCH_2CH_3$), 4.01–4.03 (t, 2H, ≡$CCH_2(CH_2)_4CH_2$O–), 6.97–6.99 (d, 4H, Ar–*H*), 7.22–7.23 (d, 2H, Ar–*H*), 7.55–7.61 (d, 6H, Ar–*H*).

4-(Methoxy)phenylboronic acid

The synthetic route is the same to 4-((*S*)-2-methylbutyl) oxyphenylboronic acid and the product was obtained as white solid. Yield: 75%. M.p.: 203–205 °C.

2-Bromo-5-(4′-methyloxyphenyl)toluene

Into a solution of 2,5-dibromotoluene (2.50 g, 0.01 mol), $Pd(PPh_3)_4$ (0.192 g), K_2CO_3 (1.38 g, 0.01 mol), H_2O (9 mL), toluene (12 mL), 4-(methoxy)phenylboronic acid (1.83 g, 0.012 mol) dissolved in 9 mL of ethanol was added dropwise at 80 °C under the protection of nitrogen. The reaction mixture was stirred for 24 h. Then the mixture was extracted with chloroform and water. The organic layer was separated, dried over anhydrous $MgSO_4$ over night, and filtered, then the solvent was distilled with a rotary evaporator. The resulting mixture was purified by column chromatography (silica gel, *n*-hexane/dichloromethane = 5). White crystals were obtained. Yield: 61.0%. M.p.: 65–67 °C.

2-[4′-((S)-2-Methylbutyl)oxyphenyl]-5-(4′-methoxyphenyl)toluene

Into a solution of 2-bromo-5-(4′-methyloxyphenyl)toluene (2.77 g, 0.01 mol), $Pd(PPh_3)_4$ (0.192 g), K_2CO_3 (1.38 g, 0.01 mol), H_2O (9 mL), toluene (12 mL), 4-((*S*)-2-methylbutyl)oxyphenylboronic acid (1.83 g, 0.012 mol) dissolved in 9 mL of ethanol was added dropwise at 80 °C under the protection of nitrogen. The reaction mixture was stirred for 24 h. After the completion of the reaction, the mixture was extracted with chloroform and water. The organic layer was separated, dried over $MgSO_4$, and filtered, then the solvent was distilled with a rotary evaporator. And the resulting mixture was purified by column chromatography (silica gel, *n*-hexane/dichloromethane = 5). White crystals. Yield: 58.3%. M.p.: 79–81 °C. ^{1}H NMR (600 MHz, $CDCl_3$-*d*, δ, ppm): 0.96–0.98 (t, 3H, –OCH_2CHCH_2–CH_3), 1.04–1.05 (d, 3H, –OCH_2CH(CH_3)–CH_2), 1.59–1.69 (m, 2H, –$OCH_2CH(CH_3)$–CH_2), 1.89–1.90 (m, 1H, –OCH_2–C*H*), 2.34 (s, 3H, Ar–CH_3), 3.78–3.80 (d, 2H, –OCH_2–$CHCH_2CH_3$), 3.86–3.87 (s, 3H, –OCH_3), 6.95–6.99 (d, 4H, Ar–*H*), 7.25–7.28 (d, 3H, Ar–*H*), 7.40–7.44 (d, 2H, Ar–*H*), 7.56–7.59 (d, 2H, Ar–*H*).

2-[4′-((S)-2-Methylbutyl)oxyphenyl]-5-(4′-methoxyphenyl)benzoic acid

2-[4′-((*S*)-2-met-hylbutyl)oxyphenyl]-5-(4′-methoxyphenyl) toluene (1.15 g, 3.2 mmol) in 19 mL of pyridine and 1.8 mL of water containing 2.0 g of potassium permanganate ($KMnO_4$) was heated at reflux for 2 h. At every 0.5 h, 3 mL of water and 1.0 g of $KMnO_4$ were added by four

times. After 5–6 h, 20 mL of water was added and kept refluxing overnight. The manganese dioxide (MnO_2) precipitate was filtered hot and washed with boiling water. The filtrate was decolored (if necessary) with active carbon and filtered through Celite. The filtrate was concentrated and the acid was recovered by addition of dilute hydrochloric acid until the PH was 3–4. The product was obtained as white power. Yield: 60.8%. M.p.: 174–176 °C.

*5-{2-[4′-((S)-2-Methylbutyl)oxyphenyl]-5-(4′-methoxyphenyl)carbonyl]oxy}-1-pentyne (**AM$_3$OCO(TPh)OR***)*

2-[4′-((*S*)-2-methylbutyl)oxyphenyl]-5-(4′-methoxyphenyl) benzoic acid (0.88 g, 2.25 mmol), 4-pentyn-1-ol (0.24 g, 2.86 mmol), *p*-toluenesulfonic (TsOH) (0.09 g, 0.53 mmol), and 4-dimethylaminopyridine (DMAP) (0.07 g, 0.55 mmol) were dissolved in 90 mL of dry CH_2Cl_2 in a 250 mL two-necked round-bottom flask under an atmosphere of nitrogen. The solution was cooled to 0–5 °C with an ice-water bath, to which 0.7 g of 1,3-dicyclohexylcarbodiimide (DCC) (3.4 mmol) in 25 mL of dichloromethane was added under stirring via a dropping funnel. The reaction mixture was stirred for 24 h. After filtering out the formed insoluble urea, the filtrate was concentrated by a rotary evaporator. The white crystals were obtained by column chromatography (silica gel, chloroform) followed by recrystallization from ethanol. Yield: 72.1%. IR (KBr, v, cm^{-1}): 2117 (C≡C), 3300 (≡CH). ^{1}H NMR (600 MHz, $CDCl_3$-*d*, δ, ppm): 0.96–0.98 (t, 3H, –OCH_2CH–CH_2–CH_3), 1.03–1.04 (d, 3H, –$OCH_2CH(CH_3)$–CH_2), 1.25–1.30 (m, 2H, –$OCH_2CH(CH_3)$–CH_2), 1.90–1.92 (m, 6H, ≡CH, ≡CCH_2, ≡CCH_2CH_2, –OCH_2–$CHCH_2CH_3$), 3.78–3.80 (d, 2H, –OCH_2–$CHCH_2$–CH_3), 3.86–3.87 (s, 3H, –OCH_3), 4.17–4.19 (t, 2H, ≡CCH_2 CH_2CH_2), 6.94–6.95 (d, 2H, Ar–*H*), 6.95–7.01 (d, 2H, Ar–*H*), 7.25–7.26 (d, 2H, Ar–*H*), 7.41–7.43 (d, 1H, Ar–*H*), 7.58–7.60 (d, 2H, Ar–*H*), 7.68–7.70 (d, 1H, Ar–*H*), 7.96 (s, 1H, Ar–*H*).

Polymerization

All the polymerization reactions and manipulations were carried out under nitrogen using Schlenk techniques in a vacuum line system or an inert atmosphere glovebox (Vacuum Atmospheres), except for the purification of the polymers. A typical experimental procedure for the polymerization of **AM$_3$OCO(TPh)OR*** was as follows.

Into a baked 20 mL Schlenk tube was added 0.456 g (1.00 mmol) of **AM$_3$OCO(TPh)OR***. The tube was evacuated under vacuum and then flushed with nitrogen three times through the sidearm. Freshly distilled THF (1.2 mL) was injected into the tube to dissolve the monomer. The catalyst solution was prepared in another tube by the dissolution of 9.3 mg of $[Rh(nbd)Cl]_2$ in mixed solution of THF (0.6 mL) and Et_3N (2.5 mL). The two tubes were aged at 60 °C for 15 min and then the monomer solution was transferred to the catalyst solution using a hypodermic syringe. The reaction mixture was stirred at 60 °C under nitrogen for 24 h. The solution was then cooled to room temperature, diluted with 3.0 mL of $CHCl_3$, and added dropwise to 500 mL of acetone through a cotton filter under stirring. The precipitate was allowed to stand overnight and then filtered with a Gooch crucible. The characterization data is as follows:

PAM$_6$OTPhOR*: Brown power. Yield: 89.3%. IR (KBr, cm^{-1}) 2950 (=C–H).

PAM$_3$OCO(TPh)OR*: Light yellow powder. Yield: 62.0%. IR (KBr, cm^{-1}) 2965 (=C–H). ^{1}H NMR (600 MHz, $CDCl_3$-*d*, δ, ppm): 0.81–2.04 (m, 13H, –OCH_2CHCH_2–CH_3, –$OCH_2CH(CH_3)$–CH_2CH_3, –OCH_2CH–CH_2, =CCH_2, =CCH_2CH_2, –OCH_2–$CHCH_2CH_3$) 3.50–4.01 (m, 7H, =$CCH_2CH_2CH_2$, –OCH_3, –OCH_2–$CHCH_2CH_3$), 4.80 (*cis* C=C*H*), 6.61–6.95 (m, 4H, Ar–*H*), 7.30–7.95 (m, 7H, Ar–*H*).

Results and discussion

Synthesis of the monomers

The synthetic routes of **AM$_6$OTPhOR*** and **AM$_3$OCO(TPh)OR*** are shown in Scheme 1. Chiral compound 4-bromo-4′-((*S*)-2-methylbutyl)oxybenzene was synthesized through the Mitsunobu etherification reaction between (*S*)-2-methyl-1-butanol and 4-bromophenol by DEAD and TPP. Then terphenyl mesogens with chiral end groups were prepared by the Suzuki coupling reaction in the presence of $Pd(PPh_3)_4$. Finally, the "side-end-fixed" type of monomer **AM$_6$OTPhOR*** and "side-on-fixed" type of **AM$_3$OCO(TPh)OR*** were obtained by the terphenyl mesogens with chiral end groups reacted with 8-bromo-1-octyne and 4-pentyn-1-ol via etherification and esterification, respectively. All of the monomers are readily dissolved in common solvents, such as THF, $CHCl_3$, and DMF, etc.

Preparation of the polymers

Transition-metal catalysts are the most commonly used catalysts for acetylene polymerizations. However, these catalysts are often found to be incapable of initiating the polymerizations of acetylene monomers containing polar functional groups, such as ether and ester units owing to the poisoning effects of the polar functional groups on the metathesis catalysts. Thus, polymerizations of monomers **AM$_6$OTPhOR*** and **AM$_3$OCO(TPh)OR*** might be a great challenge because they contain the polar ether or ester units.

A rhodium complex catalyst is known as an effective catalyst for the polymerization of monosubstituted polyacetylenes and has no poisoning interaction with monomer with FLC substituent containing the polar ether and ester group [14], we thus attempted to adopt $[Rh(nbd)Cl]_2$ in this experiment as the catalyst for polymerizations of the acetylene monomers. Polymerizations of the acetylene monomers were carried out in THF at 60 °C for 24 h. Cheerfully, both of the monomers have been polymerized and generated to their corresponding polymers in high yields. The **PAM$_3$OCO(TPh)OR**** was fusible and soluble in common organic solvents, such as THF and $CHCl_3$, and obtained moderate molecular weight (weight-average molecular weight (M_w = 23,000), number-average molecular weight (M_n = 14,300), and the molecular weight distribution (MWD, calculated by M_w/M_n is 1.60). But disappointedly, the **PAM$_6$OTPhOR**** prepared from **AM$_6$OTPhOR**** was insoluble in most common solvents, thus the molecular weight could not acquire.

Structural characterization

During the polymerization of **AM$_6$OTPhOR****, the colorless solution of the monomer **AM$_6$OTPhOR**** turned to brown color and then became more and more turbid with lengthening reaction time, implying that the resultant polymer **PAM$_6$OTPhOR**** formed aggregate. The brown aggregate could not dissolve in common organic solvents such as, $CHCl_3$, THF, toluene, and cyclohexane. The molecular characterization of **PAM$_6$OTPhOR**** became somewhat difficult because of the poor solubility. However, the FT-IR results are still adequate to support that the polymerization indeed give the desired polymer. In the spectrum of monomer **AM$_6$OTPhOR****, the ≡C–H vibration peak at about 3282 cm^{-1}, C≡C symmetry stretching vibration at 2111 cm^{-1}, and HC≡ out-of-plane vibration about 630 cm^{-1} disappear in the IR spectrum of the polymer **PAM$_6$OTPhOR****, indicating that the polymerization was conducted successfully by reaction of the opening of the triple bond. Disappearance of these peaks in the spectrum of **PAM$_3$OCO(TPh)OR**** also indicates that the alkynyl group C≡CH has been consumed.

Figure 1 shows the ^{1}H NMR (600 MHz) spectra of **AM$_6$OTPhOR****, **AM$_3$OCO(TPh)OR****, and **PAM$_3$OCO(TPh)OR**** in $CDCl_3$-*d*, except for **PAM$_6$OTPhOR**** with poor solubility, and all the resonance peaks can be readily assigned in the ^{1}H NMR spectra. It is distinct that a new peak appears in the olefin absorption region at 4.8 ppm in **PAM$_3$OCO(TPh)OR**** originating from the *cis*-olefin protons of polyene, which was absent in the spectrum of its monomer. The peak of the protons in *trans* structure at about 7.2 ppm was integrated to the peaks of aromatic protons. The *cis* content of the polymer can be calculated according to *cis* content (%) = $\{A_{cis}/[(A_{cis} + A_{total})/12]\} \times 100$, where A_{cis} and A_{total} are respectively the integrated peak areas of the absorption by the *cis* olefin proton and of the total absorption by the aromatic and *trans* olefinic protons. The *cis* content of **PAM$_3$OCO(TPh)OR**** is calculated to be 48.8% (or 51.2% *trans*). When a polymer consists of comparable amounts of *cis* and *trans* stereoisomers, it normally gives relatively broad absorption peaks because the absorbing species in the different stereochemical environments would have different chemical shifts [20]. The *cis* content of **PAM$_3$OCO(TPh)OR**** is

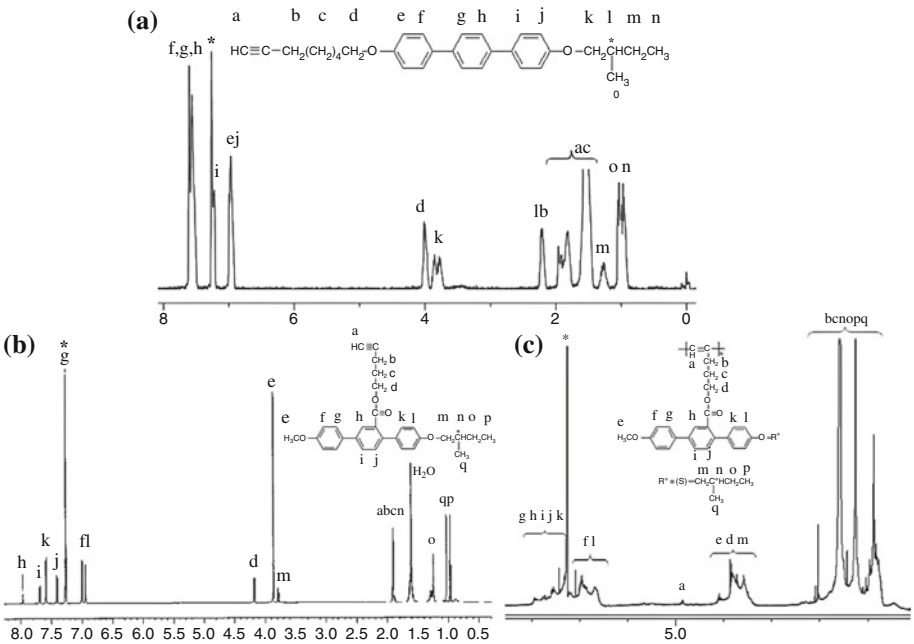

Fig. 1 ^{1}H NMR spectra of **a**, **AM$_6$OTPhOR****; **b**, **AM$_3$OCO(TPh)OR****; and **c**, **PAM$_3$OCO(TPh)OR**** with deuterated chloroform as solvent (the solvent peaks are marked with *asterisks*)

calculated to be 48.8% (or 51.2% *trans*). The polymer thus consists of comparable amounts of *cis* and *trans* stereoisomers as evidenced by its relatively broad absorption peaks. Except the peaks of solvent and water remaining in the spectrum, no unexpected signals are observed in the spectra of the products, and all the resonance peaks can be assigned to appropriate protons as marked in Fig. 1c. The ^{1}H NMR spectrum as well as the IR analyses confirms that the C≡C bond has been consumed by the polymerization reaction.

Thermal stability

Temperature for 5% mass loss has often been used as a degradation temperature (T_d) to estimate thermal stability of a synthetic polymer. From the Fig. 2, we can see that the introduction of the thermally stable mesogenic pendants into the macromolecular structures have dramatically enhanced the resistance of the polymers to thermolysis [21]. The "side-on-fixed" type of polymer **PAM$_3$OCO(TPh)OR*** (T_d = 325 °C) is more stable than "side-end-fixed" type of **PAM$_6$OTPhOR*** (T_d = 300 °C), implying that the backbone is well protected by the "jacket effect" from terphenyl mesogenic pendants linked at the waist position.

Liquid crystallinity

After checking the thermal stabilities of the polymers, we proceeded to study their mesomorphic behaviors. All the acetylene monomers and their polymers exhibited enantiotropic liquid crystalline behavior due to the introducing of terphenyl mesogens. The mesomorphic textures of the compounds are displayed in Fig. 3. All of the acetylene monomers and their polymers exhibited optical anisotropy with a birefringent texture when heated or cooled, this suggested that the terphenyl mesogens endowed the monomers and polymers with enantiotropic liquid crystalline behavior. In the first cooling program of monomer **AM$_6$OTPhOR*** from 213.2 to 201.4 °C, the fingerprint schlieren texture typical of the N* phase emerged from the dark background and grew to bigger domains. At the same time, the XRD pattern of **AM$_6$OTPhOR*** measured in the LC phase at 208 °C gave a typical pattern of a SmA type layer structure (vide post). The optical texture and the result of XRD measurement was due to **AM$_6$OTPhOR*** forming twist grain boundary smectic A (TGBA*) phase, since the TGBA* phase possesses both characteristics of the N* and smectic A phases. While the temperature was in the temperature range of 201.4–195.5 °C, a striated fanshape of SmC* phase was observed. Under further cooling, an unidentified smectic X (SmX) phase with higher ordering emerged before it solidified. As the terphenyl mesogen is linked to the main chain at the waist position, the monomer **AM$_3$OCO(TPh)OR*** is packed so well that its POM exhibited a perfect bright silk texture of chiral smectic A phase (SmA*). The **PAM$_6$OTPhOR*** exhibited fingerprint fan texture, this suggested that the mesophase of **PAM$_6$OTPhOR*** was SmC* in nature. The anisotropic entities of **PAM$_3$OCO(TPh)OR*** was growing bigger with colorful texture when cooled from isotropic liquid state, with the aid of XRD measurement, the texture was identified to be associated with SmA* phase. Both of the polymers showed the poor textures and less order than their corresponding monomers, which were probably due to the main chain string the mesogenic pendants together, making the mesogens easy to order but difficult to randomize [22].

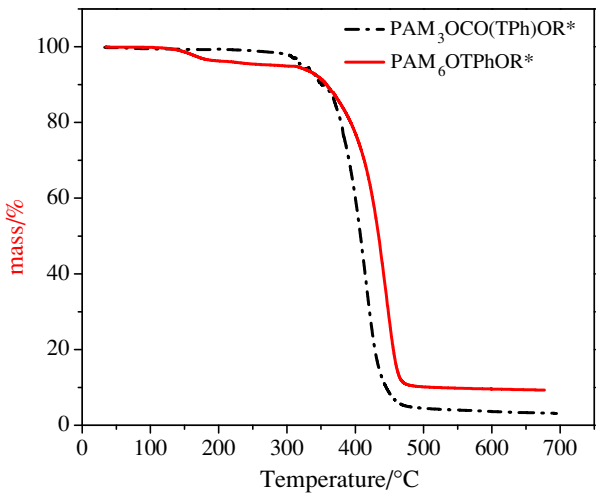

Fig. 2 TG curves of **PAM$_6$OTPhOR*** and **PAM$_3$OCO(TPh)OR*** recorded under nitrogen at a heating rate of 10 °C min^{-1}

The DSC measurement was utilized to learn more about the thermal transitions of the monomers (Fig. 4). The DSC curve of **AM$_6$OTPhOR*** showed four transition peaks at 213.2, 201.4, 195.5, 192.7 °C in the first cooling cycle, associated with the i-TGBA*, TGBA*-SmC*, SmC*-SmX*, SmX*-k transtions, respectively. Reheating the sample regenerated the SmX*, SmC*, and TGBA* phase in sequence. The DSC curve of **AM$_3$OCO(TPh)OR*** shows three transition peaks at 21.2, 53.3, and 60.1 °C in the second heating cycle. The mesophase in this temperature range (53.3–60.1 °C) was identified to be SmA* phase because silk texture of SmA* was observed. The broad exothermic peak at 21.2 °C was ascribed to recrystallization of small crystals. In the first cooling cycle, **AM$_3$OCO(TPh)OR*** entered the SmA* phase from its isotropic state at 54.7 °C and finally solidified at 40.4 °C. The "side-end-fixed" type of polymer **PAM$_6$OTPhOR*** also showed two peaks (237.2 and 226.4 °C) corresponding to i-SmC* and SmC*-g, respectively, in the first cooling scan, and the associated g-SmC* and SmC*-i transitions are observed at 236.9 and

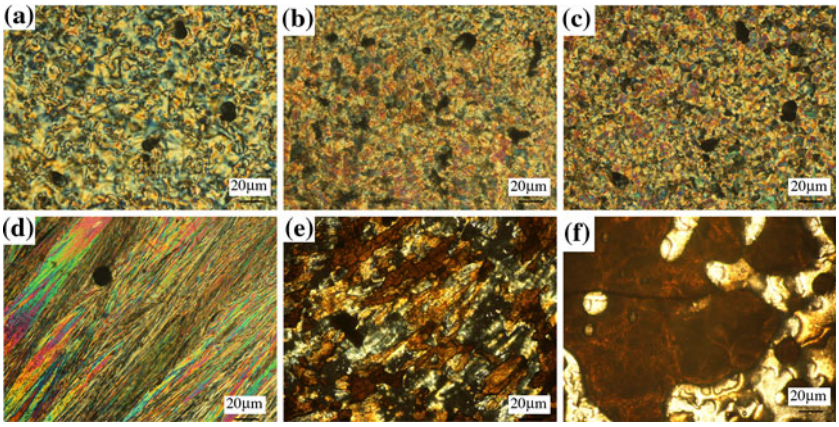

Fig. 3 Mesomorphic textures observed on cooling of **AM$_6$OTPhOR*** at **a** 203, **b** 198, and **c** 194 °C, of **AM$_3$OCO(TPh)OR*** at **d** 49.9 °C of **PAM$_6$OTPhOR*** at **e** 229 °C, and of **PAM$_3$OCO(TPh)OR*** at **f** 218 °C from their isotropic melts at a cooling rate of 1 °C min^{-1}

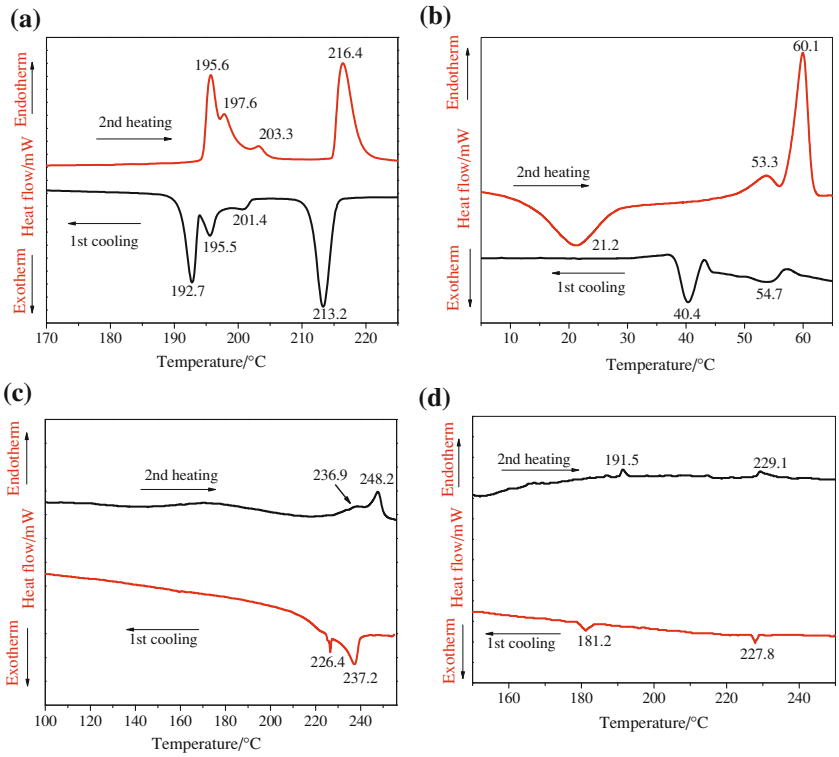

Fig. 4 DSC curves of **a**, **AM$_6$OTPhOR***; **b**, **AM$_3$OCO(TPh)OR***; **c**, **PAM$_6$OTPhOR***; and **d**, **PAM$_3$OCO(TPh)OR*** recorded under nitrogen at a scan rate of 10 °C min^{-1}

248.2 °C in the second heating scan, respectively. The transition profiles of **PAM$_3$OCO(TPh)OR*** were similar to those of **PAM$_6$OTPhOR***. In its first cooling circle, **PAM$_3$OCO(TPh)OR*** entered the SmA* phase from its isotropic state at 227.8 °C, the mesophase was stable in a temperature range over 46 °C before the polymer solidified at 181.2 °C. The peaks observed at 191.5 and 229.1 °C of the second heating cycle corresponded to the g-SmA* and SmA*-i transitions, respectively. Phase-transition temperatures of monomers and polymers are summarized in Table 1.

To verify the mesophase assignment and to learn more about the molecular packing arrangements, XRD analyses were conducted within their liquid-crystalline phases of the monomers and their polymers. Temperature-dependent XRD patterns (Fig. 5) of **AM$_6$OTPhOR*** were obtained at different liquid crystalline phases because the monomer **AM$_6$OTPhOR*** possessed three types of liquid crystalline phases observed from DSC and POM measurement. The appearance of a broad or sharp peak serves as a qualitative indication of the degree of order. All the patterns show sharp peaks at the small-angle region when cooled and heated, suggesting that the three types of liquid crystalline phases are all smectic phases. In the cooling cycle of XRD of **AM$_6$OTPhOR*** conducted at 208 °C, the sharp peak at the small-angle region was about 3° corresponding to a layer spacing d (33.34 Å), which is almost closed to the calculated molecular length of the monomer in its most extended conformation (l = 31.62 Å), thus providing a

Table 1 Thermal transition of monomers and polymers

Compound	Phase-transition temperature/°C	
	Cooling	Heating
AM$_6$OTPhOR*	i·213.2·TGBA*·201.4·SmC*·195.5·SmX*·192.7·k	k·195.6·SmX*·197.6·SmC*·203.3·TGBA*·216.4·i
AM$_3$OCO(TPh)OR*	i·54.7·SmA*·40.4·k	k·53.3·SmA*·60.1·i
PAM$_6$OTPhOR*	i·237.2·SmC*·226.4·g	g·236.9·SmC*·248.2·i
PAM$_3$OCO(TPh)OR*	i·227.8·SmA*·181.2·g	g·191.5·SmA*·229.1·i

k crystal, *g* glassy state, *SmX** unidentified chiral smectic phase, *SmC** chiral smectic C phase, *SmA** chiral smectic A phase, *TGBA** twist grain boundary smectic A* phase; *i* isotropic liquid

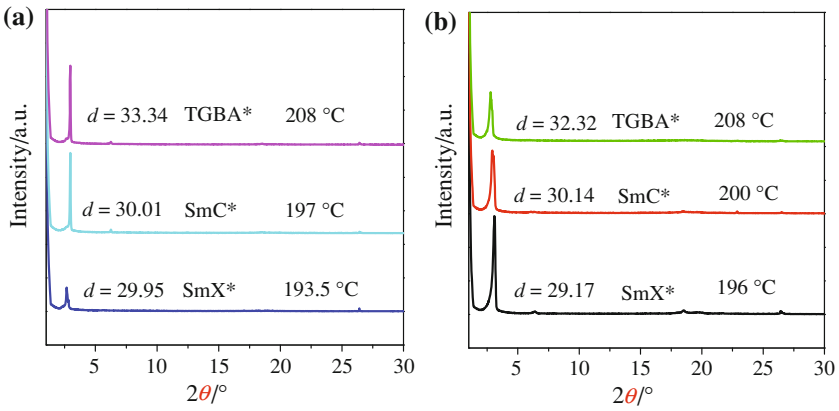

Fig. 5 Temperature-dependent XRD patterns of monomer **AM$_6$OTPhOR*** at **a** first cooling cycle and **b** second heating cycle

SmA* mesophase in a monolayer arrangement. Combining with the optical texture of N* phase, the **AM$_6$OTPhOR*** therefore formed TGBA* phase. When cooled to 197 °C, the layer spacing of the small angle reflection decreased from 33.34 to 30.01 Å, and the $d/l = 0.95$ implies that a typical SmC* was generated with a tilted formation. When the temperature was further cooled to 193.5 °C, the *d*-spacing reduced to 29.95 Å, meaning that a more ordered SmX* was developed. The liquid crystalline property of **AM$_6$OTPhOR*** was further recognized by the similar results occurred in the heating cycle of XRD. The XRD diffractogram of **AM$_3$OCO(TPh)OR*** also showed a sharp reflection at a low-angle of $2\theta = 3.38°$ proving the SmA* nature of **AM$_3$OCO(TPh)OR***. In the low-angle region, **PAM$_6$OTPhOR*** gave a Bragg reflection at $2\theta = 3.25°$. The layer thickness was calculated to be $d_1 = 26.15$ Å, which was shorter than the fully extended molecular length of the repeat unit ($l = 27.12$ Å, $d_1/l = 0.96$), this implied the monolayer structure of SmC* structure. The diffuse peak centered at $2\theta = 19.6°$ gave an average distance (d_2) of 4.54 Å associated with the lateral packing arrangement of the pendant. The proposed monolayer structure of the **PAM$_6$OTPhOR*** is described in Chart 1a. The XRD pattern of **PAM$_3$OCO(TPh)OR*** showed a Bragg reflection at $2\theta = 3.30°$ in the low-angle region, and the *d*-spacing value (26.80 Å) of the sample was almost identical to the calculated length of the rigid mesogenic units (22.54 Å), which means the side chain of the mesogenic units was perpendicular to the main chain [23]. So we presumed that the structure of the liquid-crystalline phases was bi-layer SmA*. The schematic drawing of the polymer **PAM$_3$OCO(TPh)OR*** with rigid mesogenic core is depicted in Chart 1b.

Electronic absorption and photoluminescene (PL)

The UV spectra exhibits that the **AM$_6$OTPhOR*** and **AM$_3$OCO(TPh)OR*** in THF solution can absorb UV light strongly at 298 and 290 nm, respectively, which can be assigned to π–π^* transition in the conjugated terphenyl mesogens. **PAM$_3$OCO(TPh)OR*** not only absorbs the UV light at 286 nm, but also it extends well beyond 600 nm, while none of the monomers show any peaks at wavelengths longer than 350 nm. The absorption in the long-wavelength visible spectral region is thus obviously from the backbone of the polymer.

A polymer with both liquid-crystalline and light-emitting properties may result in unique technological applications [24]. We investigate the fluorescence properties of the polymers with the aim to study the light-emitting properties. As can be seen from Fig. 6, when the wavelength of

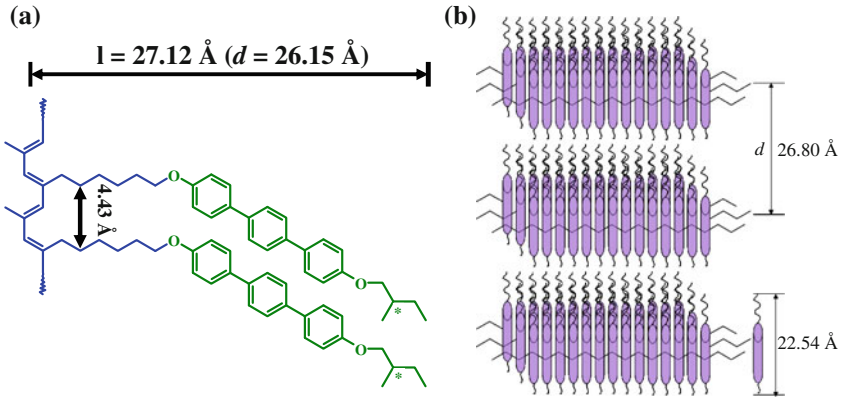

Chart 1 **a** Proposed of the **PAM$_6$OTPhOR*** within the SmC* layer with monolayer structure, **b** schematic drawing of the layer structure of the **PAM$_3$OCO(TPh)OR***

excitation light is 315 nm, **PAM$_3$OCO(TPh)OR*** in THF solution emits a strong light at 413 nm, while the light emitting band of the terphenyl mesogen is located at about 380 nm [10], so the emitting centers of the **PAM$_3$OCO(TPh)OR*** are both the chromophoric terphenyl pendant and the conjugated backbone. The UV spectra and Fig. 6 elucidate that the polyene backbone absorbs in a spectral region where its terphenyl pendant emits, therefore, the UV light emitted from the chromophoric terphenyl pendant is partially reabsorbed by the polyene backbone, suggesting that energy transfer from the terphenyl pendant to the backbone favors the stronger light-emitting of backbone. To further study the luminescence intensity of the **PAM$_3$OCO(TPh)OR***, the quantum yield (Φ_F) of the **PAM$_3$OCO(TPh)OR*** is calculated with quinine sulfate as standard induced by the 290 nm excitation is 11.54% while the quantum yield induced by the 315 nm excitation is 20.04%. This phenomenon can be explained as that the 315 nm photons can excite both the terphenyl pendant and the polyene backbone, reasonably, the direct excitation plus

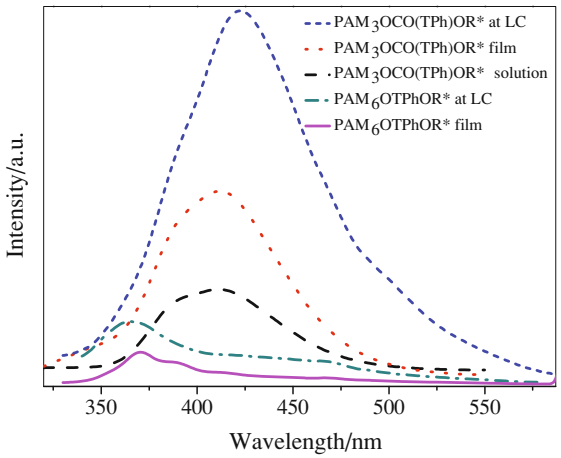

Fig. 6 Photoluminescence spectra of the **PAM$_6$OTPhOR*** and **PAM$_3$OCO(TPh)OR*** in different states. Excitation wavelength: 315 nm

the energy transferred from the terphenyl pendant leading to the more efficient emission of **PAM$_3$OCO(TPh)OR*** induced by the longer wavelength excitation, while the 290 nm photons mainly excite the terphenyl pendant [10]. The reliable light-emitting property of **PAM$_6$OTPhOR*** in solution was not obtained due to its poor solubility.

Many conjugated polymers emit intensely in solution but become weak emitters when fabricated into films resulting from the forming less luminescent species [25, 26]. In order to check out whether the same phenomenon happened in our polymer **PAM$_3$OCO(TPh)OR***, the film was prepared to check its fluorescence property. Delightfully, the PL spectra reveal that the polymer emitted remarkably stronger in film than that in THF solution, and no significant shift in the peak maximum is observed in comparison to that in the solution, indicating that the polymer remains emissive in the aggregation. This is suggestive of little excimer absorption and emission, and the segregation of the backbone by the bulky terphenyl mesogen pendants effectively decreases the strong interchain interaction.

The spontaneous orientation of the mesogenic group of polymer and the molecular arrangement can be readily manipulated by external forces [27, 28]. Especially for FLC, their spontaneous polarization is a crucial factor for quickly responding to the electric field. Thus, the effects of the spontaneous orientation of the mesogenic group on the light-emitting of the polymers at the liquid crystalline states have also been investigated. The patterns of the polymers were obtained at room temperature after the samples had been quenched from liquid-crystalline states with liquid nitrogen. In Fig. 6, the light-emitting band of the both polymers in the liquid crystalline states are stronger and red-shifted to the long wavelength region compared to those of the thin film state due to the increasing conjugation length along the main chains in the LC states. For **PAM$_3$OCO(TPh)OR***, the light-emitting of liquid crystalline state is two times stronger than that of its thin film, and even extend to near 600 nm. This demonstrates that the enhanced spontaneous orientation of the terphenyl mesogens at the LC states could

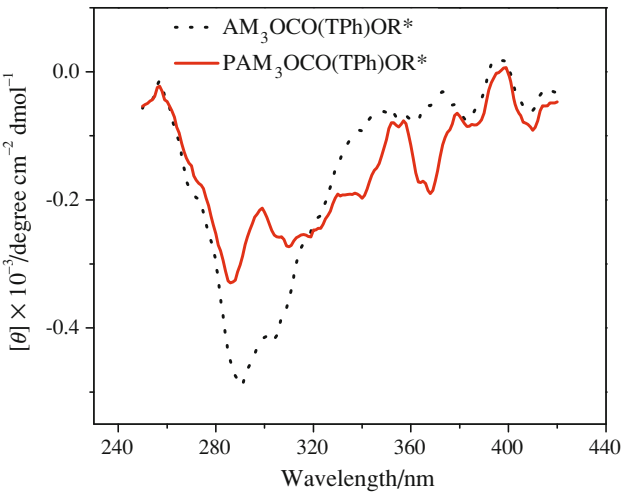

Fig. 7 The CD spectra of **AM$_3$OCO(TPh)OR*** and **PAM$_3$OCO(TPh)OR*** measured in THF solution (c = 0.25 mM)

effectively improve the main-chain orientation, resulting in improved photoluminescene properties. **PAM6OTPhOR*** in both film and LC states show a band at about 370 nm due to the existence of the terphenyl side chain, but it shows a little partial band attributed to the main chain. This may be due to a weak conjugation on the backbone.

Compared to that of "side-end-fixed" polymer **PAM6OTPhOR***, the light-emitting bands of "side-on-fixed" polymer **PAM3OCO(TPh)OR*** in both film and LC state are much stronger and about 50 nm red-shifted, indicating that the steric effect of the bulk terphenyl mesogenic pendants linked at the waist position have stronger tendency to enhance the main-chain coplanarity than the "side-end-fixed" type.

Helix structure of the polymer **PAM$_3$OCO(TPh)OR***

Akagi and coworkers found that the chiroptical properties of the chiral pendants were maintained after polymerization, but helical backbone conformation was not detected [14]. Here, polymer **PAM3OCO(TPh)OR*** is easily soluble in many common organic solvents, allowing us to investigate its properties by "wet" spectroscopic methods. The CD spectra of monomer **AM$_3$OCO(TPh)OR*** and its polymer **PAM$_3$OCO(TPh)OR*** in dilute THF solution are listed in Fig. 7. Compared with the absorption of monomer **AM$_3$OCO(TPh)OR***, there is a similar broad band from 257 to 350 nm, so we can speculate that the band in CD located 257–350 nm is ascribed to the absorption band of chiroptical terphenyl group, this suggests the chiroptical property of the terphenyl pendant was maintained after polymerization. The spectrum of polymer **PAM$_3$OCO(TPh)OR*** also exhibit a new band from 357 to 379 nm relative to its monomer, which shall be attributed to π–π^* electronic transition of the polyene backbone. And the relatively strong Cotton effect observed at 369 nm clearly indicates the existence of backbone containing a helical conformation with an excess of single-handedness. This confirms that the asymmetric force field generated by the chiral center indeed affects the secondary structure of **PAM$_3$OCO(TPh)OR*** [29]. The CD spectrum of **PAM$_6$OTPhOR*** wasn't detected resulting from its poor solubility.

Summary

In this study, we have successfully synthesized novel FLC polyacetylenes (**PAM$_6$OTPhOR*** and **PAM$_3$OCO(TPh)OR***) containing terphenyl pendants with chiral end groups. Using $[Rh(nbd)Cl]_2$ catalyst generated the polymers with high yields. Disappointedly, "side-end-fixed" type of polymer **PAM$_6$OTPhOR*** was insoluble in common solvents, while **PAM$_3$OCO(TPh)OR*** show excellent solubility in most solvents. The thermal stability of two polymers are higher than 300 °C, it is intriguing to note that the T_d of **PAM$_3$OCO(TPh)OR*** is much higher than **PAM$_6$OTPhOR***, owing to the "jacket effect" from terphenyl mesogenic pendants linked at the waist position better protecting the main-chain from the perturbations. Thanks to the terphenyl mesogenic pendants, the monomers and polymers are all liquid crystalline and exhibit enantiotropic mesophases when heated or cooled. It is noteworthy that the "side-end-fixed" type of **PAM$_6$OTPhOR*** showed enantiotropic SmC* responsible for ferroelectric liquid crystallity. The polymers in their liquid crystalline states show better PL properties than in both solution and film states. What's more, the CD spectrum of the polymer **PAM$_3$OCO(TPh)OR*** shows that the polymer not only maintains the chiroptical property of the monomers, but also takes one-handed helical structure of the backbone.

Acknowledgements This work was supported by the National Natural Science Foundation of China (51073076, 50902067 and 51003045).

References

1. Katz HE. Organic molecular solids as thin film transistor semiconductors. J Mater Chem. 1997;7:369–75.
2. Burroughes JH, Bradley DDC, Brown AR, Marks RN, Mackay K, Friend KH, Burn PL, Kraft A, Holmes AB. Light-emitting diodes based on conjugated polymers. Nature. 1990;347:539–41.
3. Lüessem G, Festag R, Greiner A, Schmidt C, Unterlechner C, Heitz W, Wendorff JH, Hopmeier M, Feldmann J. Polarized photoluminescence of liquid crystalline polymers with isolated arylenevinylene segments in the main chain. Adv Mater. 1995;7:923–5.

4. Chen SH, Conger BM, Mastrangelo JC, Kende AS, Kim DU. Synthesis and optical properties of thermotropic polythiophene and poly(p-phenylene) derivatives. Macromolecules. 1998;31: 8051–7.
5. Yoshino K, Yin XH, Morita S, Nakazono M, Kawai T, Ozaki M, Jin SH, Choi SK. Unique electrical and optical properties of conducting polymeric liquid crystal. Jpn J Appl Phys (Part 2). 1993;32:L1673–6.
6. Nagai K, Masuda T, Nakagawa T, Freeman BD, Pinnau I. Poly [1-(trimethylsilyl)-1-propyne] and related polymers: synthesis, properties and functions. Prog Polym Sci. 2001;26:721–98.
7. Liu JZ, Lam JWY, Tang BZ. Acetylenic polymers: syntheses, structures, and functions. Chem Rev. 2009;109:5799–867.
8. Akagi K. Synthesis and properties of liquid-crystalline-conjugated polymers. Bull Chem Soc Jpn. 2007;80:649–61.
9. Radhakrishnan S, Somanathan N, Narashimhaswamy T, Thelakkat M, Schmidt HW. Thermal studies on polythiophene containing mesogenic side chains. J Therm Anal Calorim. 2006; 85:433–8.
10. Chen L, Chen YW, Zhou D, Li F, Zha DJ, Yao K. Enhanced photoluminescence, mesomorphism and conformation of liquid-crystalline conjugated polymers with terphenyl mesogen pendants. Macromol Chem Phys. 2011;212:24–41.
11. Zhou QF, Li HM, Feng XD. Synthesis of liquid-crystalline polyacrylates with laterally substituted mesogens. Macromolecules. 1987;20:233–4.
12. Yao YH, Yang SH, Hsu CS. Synthesis of laterally attached side-chain liquid crystalline poly(p-phenylene vinylene) and polyfluorene derivatives for the application of polarized electroluminescence. Polymer. 2006;47:8297–308.
13. Dai XM, Goto H, Akagi K, Shirakawa H. Synthesis and properties of novel ferroelectric liquid crystalline polyacetylene derivatives. Synth Met. 1999;102:1289–90.
14. Goto H, Dai XM, Ueoka T, Akagi K. Synthesis and properties of polymers from monosubstituted acetylene derivatives bearing ferroelectric liquid crystalline groups. Macromolecules. 2004;37: 4783–93.
15. Goto H, Dai XM, Narihiro H, Akagi K. Synthesis of polythiophene derivatives bearing ferroelectric liquid crystalline substituents. Macromolecules. 2004;37:2353–62.
16. Oguma J, Dai XM, Akagi K. Synthesis and properties of ferroelectric liquid crystalline poly(p-phenylenevinylene) derivatives. Mol Cryst Liq Cryst. 2001;365:331–8.
17. Suda K, Akagi K. Electro-optical behavior of ferroelectric liquid crystalline polyphenylene derivatives. J Polym Sci A Polym Chem. 2008;46:3591–610.
18. Goulding M, Greenfield S, Parri O, Coates D. Liquid crystals with a thiomethyl end group: lateral fluoro substituted 4-(trans-4-(n-propyl)cyclohexylethyl)-4′-thiomethylbiphenyls and 4-n-alkyl-4″-thiomethylterphenyls. Mol Cryst Liq Cryst. 1995;265: 2593–606.
19. Chen L, Chen YW, Zhou WH, He XH, Song YL, Zhang ZJ. Synthesis and thermal analysis of disubstituted propiolates bearing terphenylene mesogen. J Therm Anal Calorim. 2010;99: 391–7.
20. Masuda T, Higashimura T. Synthesis of high polymers from substituted acetylenes: exploitation of molybdenum- and tungsten-based catalysts. Acc Chem Res. 1984;17:51–6.
21. Tang BZ. Optically active polyacetylenes: helical chirality and biomimetic hierarchical structures. Polym News. 2001;26: 262–72.
22. Yuan WZ, Qin A, Lam JWY, Sun JZ, Dong YQ, Haeussler M, Liu JZ, Xu HP, Zheng Q, Tang BZ. Disubstituted polyacetylenes containing photopolymerizable vinyl groups and polar ester functionality: polymer synthesis, aggregation-enhanced emission, and fluorescent pattern formation. Macromolecules. 2007;40: 3159–66.
23. Chen S, Gao LC, Zhao XD, Chen XF, Fan XH, Xie PY, Zhou QF. Synthesis and properties of mesogen-jacketed liquid crystalline polymers with asymmetry mesogenic core. Macromolecules. 2007;40:5718–25.
24. O'Neill M, Kelly SM. Liquid crystals for charge transport, luminescence, and photonics. Adv Mater. 2003;15:1135–46.
25. Li YN, Vamvounis G, Holdcroft S. Tuning optical properties and enhancing solid-state emission of poly(thiophene)s by molecular control: a postfunctionalization approach. Macromolecules. 2002;35:6900–6.
26. Grell M, Bradley DDC, Ungar G, Hill J, Whitehead KS. Interplay of physical structure and photophysics for a liquid crystalline polyfluorene. Macromolecules. 1999;32:5810–7.
27. Geng JX, Zhao XG, Zhou E, Li G, Lam JWY, Tang BZ. Shear induced molecular alignments of a side-chain liquid crystalline polyacetylene containing biphenyl mesogens. Polymer. 2003;44: 8095–102.
28. Geng JX, Zhou E, Li G, Lam JWY, Tang BZ. Electric field-induced molecular alignment of side-chain liquid-crystalline polyacetylenes containing biphenyl mesogens. J Polym Sci B Polym Phys. 2004;42:1333–41.
29. Liu JH, Yan JJ, Chen EQ, Lam JWY, Dong YP, Liang DH, Tang BZ. Chain helicity of a poly(phenylacetylene) with chiral centers between backbone and mesogenic groups on side chains. Polymer. 2008;49:3366–70.